Journal of Systems Engineering and Electronics
Vol. 31, No. 6, December 2020, pp.1140 – 1151

TDOA and track optimization of UAV swarm based on D-optimality

ZHOU Ronghua, SUN Hemin, LI Hao*, and LUO Weilin

Department of Intelligence, Air Force Early Warning Academy, Wuhan 430019, China

Abstract: To solve the problem of time difference of arrival (TDOA) positioning and tracking of targets by the unmanned aerial vehicles (UAV) swarm in future air combat, this paper adopts the TDOA positioning method and uses time difference sensors of the UAV swarm to locate target radiation sources. Firstly, a TDOA model for the target is set up for the UAV swarm under the condition that the error variance varies with the received signal-to-noise ratio. The accuracy of the positioning error is analyzed by geometric dilution of precision (GDOP). The D-optimality criterion of the positioning model is theoretically derived. The target is positioned and settled, and the maximum value of the Fisher information matrix determinant is used as the optimization objective function to optimize the track of the UAV in real time. Simulation results show that the track optimization improves the positioning accuracy and stability of the UAV swarm to the target.

Keywords: time difference of arrival (TDOA), unmanned aerial vehicles (UAV) swarm, D-optimality, track optimization.

DOI: 10.23919/JSEE.2020.000086

1. Introduction

American scholars John Aquila and David Longfield once pointed out in their monographs "Swarm and the Future of Conflict" that in the future battlefield, "swarm war" will become the fourth war in human history after "melee war", "assembly war" and "mobile war" [1,2]. Faced with a highly confrontational, uncertain and dynamic battlefield environment, the unmanned aerial vehicles (UAV) combat style has gradually developed from single platform operation to multi-platform "swarm" operation [3]. In future operations, the primary task of the UAV swarm is to solve the perception problem in observation, orientation, decision, action (OODA) ring. In radar-based situation awareness, passive location equipment benefits from its small size, light weight, low probability of being found by the enemy, and is more suitable for task loading of current UAV swarm.

According to the location system, the passive location system can be divided into the angle of arrival (AOA) [4–6], time of arrival (TOA) [7−9], time difference of arrival (TDOA) [10−12] and the received single strength (RSS) [13–15], etc. Among them, the TDOA positioning is widely used because it does not require strict time synchronization between the target and the positioning base station, and the positioning accuracy is high. The TDOA positioning is also called hyperbolic positioning. Its core is to solve the nonlinear positioning equations. The main methods include the iterative method, the search method and the analytical method. Among them, the iterative method [16] includes the Gauss-Newton method [17] and Newton Raphson method. Its basic idea is to obtain the estimated value through the Taylor expansion of the estimated parameter, and then use the least square to estimate the correction, and then repeat the iteration. The basic idea of the search method is to traverse the target function corresponding to the value of the estimated value, and obtain the optimal value satisfying the constraint through the search, which is the final estimated value of the estimated value. The solution method is mainly based on intelligent algorithms [18], such as the particle swarm algorithm, the ant colony algorithm, and the genetic algorithm. The characteristic of the analytical method is that the analytical expression of the target parameters to be estimated is derived by simultaneous nonlinear observation equations and approximate pseudo linearization, mainly including the Chan algorithm [19], the spherical intersection (SX) method [20], and the spherical interpolation (SI) method [21]. In this paper, when solving the TDOA equation, considering the need of real-time planning of the UAV's track, the Chan algorithm with high positioning accuracy and fast calculation speed is adopted.

Manuscript received March 19, 2020.

*Corresponding author.

This work was supported by the National Natural Science Foundation of China (61502522), the Equipment Pre-Research Field Fund (JZX7Y20190253036101), the Equipment Pre-Research Ministry of Education Joint Fund (6141A02033703), and the Hubei Provincial Natural Science Foundation (2019CFC897).

According to the number of location base stations, passive location can be divided into single station passive location and multi-station passive location [22−24]. For the multi-station passive location, the research of the fixed base station for static target location and the fixed base station for moving target location is relatively mature, and the layout of the location base station will greatly affect the final positioning accuracy. Therefore, it is extremely important to improve the positioning accuracy of moving targets by real-time planning of the UAV's track according to the moving state of the targets to achieve a reasonable layout. Frew and Semper et al. gave the path planning of UAV with different positioning methods [25,26], the core of which was to establish the optimal criteria for target positioning. Frew et al. [25] used the signal strength of the target radiation source to control the movement of the UAV, and Semper et al.[26] used the position dilution of precision (PDOP) as the criterion to control the speed and direction of the UAV. In [27], the path planning method was preliminarily studied when there was only one base station moving in the process of TDOA positioning.

The main contribution of this paper is to establish the TDOA localization model of distance-dependent noise, which is different from the general TDOA localization model in which the receiver noise is Gaussian noise, and the model in this paper is closer to the actual situation. Secondly, by solving the Fisher information matrix [28] of various angles of TDOA in the next time, the angle corresponding to the maximum determinant is taken as the flight direction of each UAV in the next time, and the flight path of the UAV swarm is planned in real time.

2. Problem modeling

2.1 TDOA localization model

It is assumed that the target radiation source in the space is located at $\boldsymbol{p}(x,y)\in\mathbf{R}^2$, and the positions of n positioning base stations are $\boldsymbol{Q}=[\boldsymbol{q}_1,\boldsymbol{q}_2,\cdots,\boldsymbol{q}_n]\in\mathbf{R}^{2\times n}$, $n\geqslant 2$, where $\boldsymbol{q}_1$ is the reference base station. There is no time synchronization between the target and the UAV base station, while the time between the UAV base stations is synchronous. There are the following positioning equations:

$$\boldsymbol{t}=\boldsymbol{t}^0+\boldsymbol{\omega} \tag{1}$$

where $\boldsymbol{t}=[t_{21},t_{31},\cdots,t_{i1},\cdots,t_{n1}]^{\mathrm{T}}$, $\boldsymbol{t}^0=\left[t_{21}^0,t_{31}^0,\cdots,t_{i1}^0,\cdots,t_{n1}^0\right]^{\mathrm{T}}$ is the real value of the time difference excluding noise, t_{i1} is the time difference between the signal arriving at the ith base station and the reference base station.

$$\boldsymbol{\omega}=[\ \omega_{21},\ \omega_{31},\ \cdots,\ \omega_{n1}\ ]^{\mathrm{T}}=\begin{bmatrix}-1&1&0&\cdots&0\\-1&0&1&\cdots&0\\\vdots&\vdots&\vdots&\ddots&\vdots\\-1&0&0&\cdots&1\end{bmatrix}\begin{bmatrix}\omega_1\\\omega_2\\\\\vdots\\\omega_n\end{bmatrix} \tag{2}$$

where ω_i follows an independent Gaussian distribution with a mean value of 0 and a variance of σ^2, the covariance matrix of the noise vector can be obtained as

$$\boldsymbol{\Omega}=\sigma^2(\boldsymbol{I}+\boldsymbol{\Phi}) \tag{3}$$

where $\boldsymbol{I}$ is the identity matrix of $(n-1)\times(n-1)$, and $\boldsymbol{\Phi}$ is a matrix of all ones.

TDOA positioning is to use the obtained time difference matrix $\boldsymbol{t}$ and base station coordinates $\boldsymbol{Q}$ to locate the target radiation source.

2.2 Distance-dependent noise model

The true value of TOA measurement error variance is not a fixed value, but is related to the signal parameters of each receiver [29,30]. Considering the influence of signal frequency, bandwidth, signal-to-noise ratio (SNR), etc, the error variance σ^2 of the TOA measurement can be expressed [31−33] as

$$\sigma_i^2\geqslant\frac{\alpha^2}{\mathrm{SNR}_i\cdot B^2} \tag{4}$$

where B is the signal bandwidth, SNR_i is the (SNR) of the ith UAV, and α is some constant. In the case where the received signal bandwidth is constant, the received measurement error is related to the SNR of the received signal. When the radiated power and the frequency are constant, the SNR is mainly determined by the distance between the receiver and the target. Therefore, the variation relationship between the error and the distance of the ith receiver can be expressed as

$$\sigma_i^2(s)=\begin{cases}\dfrac{\beta}{\mathrm{SNR}_0}\cdot\dfrac{s_i^2}{s_0^2}, & s_i>s_0\\[2ex]\dfrac{\beta}{\mathrm{SNR}_0}, & s_i\leqslant s_0\end{cases} \tag{5}$$

where s_0 is the distance lower bound corresponding to the minimum error variance of the TOA, and SNR_0 is the corresponding SNR. When $s_i>s_0$, $\sigma_i^2(s)$ is proportional to s_i; when $s_i\leqslant s_0$, the magnitude of the error no longer varies with distance.

3. Positioning accuracy analysis

The positioning accuracy is usually measured by the geometric dilution of precision (GDOP). The smaller the GDOP value, the higher the positioning accuracy. The GDOP of the four-station passive TDOA positioning [34] is

$$\text{GDOP} = \sqrt{\delta_x^2 + \delta_y^2 + \delta_z^2} \tag{6}$$

where δ_x^2, δ_y^2, δ_z^2 represent the standard deviations of the positioning in the x, y, z directions.

Differentiate both sides of $\Delta r_i = r_i - r_1$ and simplify

$$\begin{aligned} \mathrm{d}(\Delta r_i) = (c_{ix} - c_{1x})\mathrm{d}x + (c_{iy} - c_{1y})\mathrm{d}y + \\ (c_{iz} - c_{1z})\mathrm{d}z + (k_i - k_1) \end{aligned} \tag{7}$$

where Δr_i represents the distance difference, $i = 2, 3, 4$,

$$\begin{cases} r_i^2 = (x - x_i)^2 + (y - y_i)^2 + (z - z_i)^2 \\ r_1^2 = (x - x_1)^2 + (y - y_1)^2 + (z - z_1)^2 \end{cases}$$

$$\begin{cases} c_{ix} = \dfrac{\partial r_i}{\partial x} = -\dfrac{\partial r_i}{\partial x_i} = \dfrac{x - x_i}{r_i} \\ c_{iy} = \dfrac{\partial r_i}{\partial y} = -\dfrac{\partial r_i}{\partial y_i} = \dfrac{y - y_i}{r_i} \\ c_{iz} = \dfrac{\partial r_i}{\partial z} = -\dfrac{\partial r_i}{\partial z_i} = \dfrac{z - z_i}{r_i} \\ k_i = c_{ix}\mathrm{d}x_i + c_{iy}\mathrm{d}y_i + c_{iz}\mathrm{d}z_i \end{cases} . \tag{8}$$

Written in vector form:

$$\mathrm{d}\Delta\boldsymbol{R} = \boldsymbol{C}\mathrm{d}\boldsymbol{R} + \mathrm{d}\boldsymbol{S} \tag{9}$$

where $\mathrm{d}\Delta\boldsymbol{R} = [\mathrm{d}\Delta r_2, \mathrm{d}\Delta r_3, \mathrm{d}\Delta r_4]^{\mathrm{T}}$ is the error introduced by the measurement of the difference in TOA at each station, $\mathrm{d}\boldsymbol{R}=[\mathrm{d}x, \mathrm{d}y, \mathrm{d}z]^{\mathrm{T}}$ is the position error of the requested radiation source, $\mathrm{d}\boldsymbol{S}=[k_2 - k_1, k_3 - k_1, k_4 - k_1]^{\mathrm{T}}$ is the error introduced by each station site measurement,

$$\boldsymbol{C} = \begin{bmatrix} \dfrac{x - x_2}{r_2} - \dfrac{x - x_1}{r_1} & \dfrac{y - y_2}{r_2} - \dfrac{y - y_1}{r_1} & \dfrac{z - z_2}{r_2} - \dfrac{z - z_1}{r_1} \\ \dfrac{x - x_3}{r_3} - \dfrac{x - x_1}{r_1} & \dfrac{y - y_3}{r_3} - \dfrac{y - y_1}{r_1} & \dfrac{z - z_3}{r_3} - \dfrac{z - z_1}{r_1} \\ \dfrac{x - x_4}{r_4} - \dfrac{x - x_1}{r_1} & \dfrac{y - y_4}{r_4} - \dfrac{y - y_1}{r_1} & \dfrac{z - z_4}{r_4} - \dfrac{z - z_1}{r_1} \end{bmatrix}$$

is the correlation coefficient matrix between the site location and the target.

Use the least square method to solve the positioning error value:

$$\mathrm{d}\boldsymbol{R} = \left(\boldsymbol{C}^{\mathrm{T}}\boldsymbol{C}\right)^{-1}\boldsymbol{C}^{\mathrm{T}}(\mathrm{d}\Delta\boldsymbol{R} - \mathrm{d}\boldsymbol{S}). \tag{10}$$

Let $\boldsymbol{B} = (\boldsymbol{C}^{\mathrm{T}}\boldsymbol{C})^{-1}\boldsymbol{C}^{\mathrm{T}}=[b_{ij}]_{3\times 3}$, (10) can be expressed as

$$\mathrm{d}\boldsymbol{R} = \boldsymbol{B}(\mathrm{d}\Delta\boldsymbol{R} - \mathrm{d}\boldsymbol{S}). \tag{11}$$

It can be known from the above formula that the time error $\mathrm{d}\Delta\boldsymbol{R}$ and the positioning error $\mathrm{d}\boldsymbol{R}$ of the radiation source, the position of the radiation source relative to each station, and the site error $\mathrm{d}\boldsymbol{S}$ are related [35].

The time difference used in the above formula is the time difference between the arrival of the radiation source at each auxiliary station and the main station. Therefore, the time measurement error includes the measurement amount of the main station, and the time difference measurement error between the stations is related. Assuming that the station measurement error is constant throughout the process and the station measurement errors at each station are independent of each other, the covariance of the positioning errors is

$$\begin{aligned} \boldsymbol{P}_{\mathrm{d}\boldsymbol{R}} = \mathrm{E}\left\{\mathrm{d}\boldsymbol{R}\cdot\mathrm{d}\boldsymbol{R}^{\mathrm{T}}\right\} = \\ \boldsymbol{B}\left\{\mathrm{E}\left\{\mathrm{d}\Delta\boldsymbol{R}\cdot\mathrm{d}\Delta\boldsymbol{R}^{\mathrm{T}}\right\} + \mathrm{E}\left\{\mathrm{d}\boldsymbol{S}\cdot\mathrm{d}\boldsymbol{S}^{\mathrm{T}}\right\}\right\}\boldsymbol{B}^{\mathrm{T}}, \end{aligned} \tag{12}$$

$$\mathrm{E}\left\{\mathrm{d}\boldsymbol{R}\cdot\mathrm{d}\boldsymbol{R}^{\mathrm{T}}\right\} = \begin{bmatrix} \delta_{\Delta r_2}^2 & \eta_{23}\delta_{\Delta r_2}\delta_{\Delta r_3} & \eta_{24}\delta_{\Delta r_2}\delta_{\Delta r_3} \\ \eta_{23}\delta_{\Delta r_2}\delta_{\Delta r_3} & \delta_{\Delta r_3}^2 & \eta_{34}\delta_{\Delta r_2}\delta_{\Delta r_3} \\ \eta_{24}\delta_{\Delta r_2}\delta_{\Delta r_3} & \eta_{34}\delta_{\Delta r_2}\delta_{\Delta r_3} & \delta_{\Delta r_4}^2 \end{bmatrix}, \tag{13}$$

$$\begin{aligned} \mathrm{E}\{\mathrm{d}\boldsymbol{S}\cdot\mathrm{d}\boldsymbol{S}^{\mathrm{T}}\} = \begin{bmatrix} C_{2x}^2\delta_{x_2}^2 + C_{2y}^2\delta_{y_2}^2 + C_{2z}^2\delta_{z_2}^2 & 0 & 0 \\ 0 & C_{3x}^2\delta_{x_3}^2 + C_{3y}^2\delta_{y_3}^2 + C_{3z}^2\delta_{z_3}^2 & 0 \\ 0 & 0 & C_{4x}^2\delta_{x_4}^2 + C_{4y}^2\delta_{y_4}^2 + C_{4z}^2\delta_{z_4}^2 \end{bmatrix} + \\ \left(C_{1x}^2\delta_{x_1}^2 + C_{1y}^2\delta_{y_1}^2 + C_{1z}^2\delta_{z_1}^2\right)\begin{bmatrix} 1 & 1 & 1 \\ 1 & 1 & 1 \\ 1 & 1 & 1 \end{bmatrix}, \end{aligned} \tag{14}$$

where $\delta_{\Delta r_i}^2$ is the standard deviation of the measurement error of the distance difference between the ith station and the master station, and η_{ij} is the correlation coefficient between Δr_i and Δr_j:

$$\eta_{ij} = \frac{\mathrm{cov}(\Delta r_i, \Delta r_j)}{\delta_{\Delta r_i}\delta_{\Delta r_j}}. \tag{15}$$

$\delta_{x_i}^2$, $\delta_{y_i}^2$, $\delta_{z_i}^2$ are the standard deviations of the components of the site error. Since the engineering information of the site location is given by global positioning system (GPS) in actual engineering, it can be considered that the components are the same, and $\delta_{x_i}^2=\delta_{y_i}^2=\delta_{z_i}^2=\delta_s^2$ is obtained, because $c_{ix}^2+c_{iy}^2+c_{iz}^2=1$ is substituted into (14).

$$\mathrm{E}\left\{\mathrm{d}\boldsymbol{R}\cdot\mathrm{d}\boldsymbol{R}^{\mathrm{T}}\right\}=\begin{bmatrix}2\delta_s^2 & \delta_s^2 & \delta_s^2\\ \delta_s^2 & 2\delta_s^2 & \delta_s^2\\ \delta_s^2 & \delta_s^2 & 2\delta_s^2\end{bmatrix} \tag{16}$$

Let $\left[\delta_{ij}^2\right]_{3\times3}=\mathrm{E}\{\mathrm{d}\Delta\boldsymbol{R}\cdot\mathrm{d}\Delta\boldsymbol{R}^{\mathrm{T}}\}+\mathrm{E}\{\mathrm{d}\boldsymbol{S}\cdot\mathrm{d}\boldsymbol{S}^{\mathrm{T}}\}$. Substituting (10) and (13) into the above formula gives

$$\delta_{ij}^2=\begin{cases}\delta_{\Delta r_i}^2+2\delta_s^2, & i=j\\ \eta_{ij}\delta_{\Delta r_i}+\delta_s^2, & i\neq j\end{cases} \tag{17}$$

where $i, j=1,2,3$.

Let $\boldsymbol{P}_{\mathrm{d}\boldsymbol{R}}=\left|P_{ij}\right|_{3\times3}$,

$$P_{ij}=\sum_{k=1}^{3}\sum_{l=1}^{3}b_{ik}b_{jl}\delta_{kl}^2,\quad i,j=1,2,3. \tag{18}$$

From this, the variances of the positioning errors in the x, y and z directions are

$$\begin{cases}\delta_x^2=P_{11}\sum\limits_{k=1}^{3}\sum\limits_{l=1}^{3}c_{1k}b_{1l}\delta_{kl}^2\\ \delta_y^2=P_{22}\sum\limits_{k=1}^{3}\sum\limits_{l=1}^{3}c_{2k}b_{2l}\delta_{kl}^2\\ \delta_z^2=P_{33}\sum\limits_{k=1}^{3}\sum\limits_{l=1}^{3}c_{3k}b_{3l}\delta_{kl}^2\end{cases} \tag{19}$$

$$\mathrm{GDOP}=\sqrt{\delta_x^2+\delta_y^2+\delta_z^2}=\sqrt{\sum_{i=1}^{3}\sum_{j=1}^{3}(c_{1k}c_{1l}+c_{2k}c_{2l}+c_{3k}c_{3l})\delta_{kl}^2}\,. \tag{20}$$

Typical station layout methods include Y-type, T-type, and diamond Fig. 1 shows the schematic diagram of different station lagout methods. Factors such as the baseline length, measurement error, and site error of the station layout also affect the positioning accuracy. To improve the positioning accuracy of the target, it is the key to choose the optimal layout scheme. The three typical station layout methods are analyzed below.

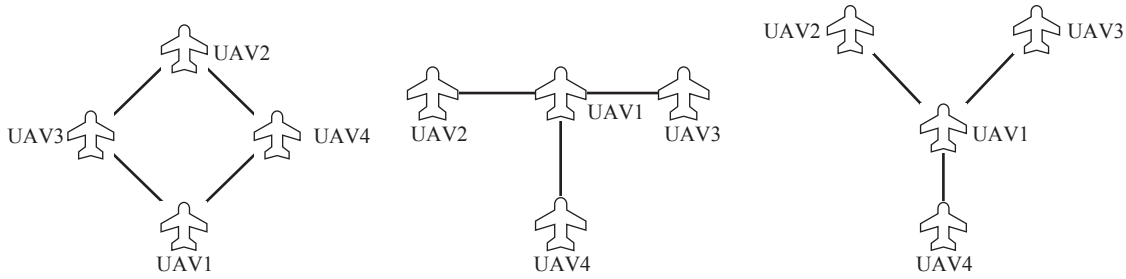

Fig. 1 Station layout

Different layout methods correspond to different positioning errors. The coordinates of the four layouts of the diamond, T and Y are shown in Table 1, Table 2 and Table 3. Table 1 is the layout of the base station with a baseline length of 10 km. Table 2 shows the coordinates of the four stations with a baseline length of 20 km, and Table 3 shows the coordinates of the four stations with a baseline length of 30 km. Set the test accuracy to 5 ns.

After the simulation, the positioning error GDOP maps as shown in Figs. 2−4 are obtained. Fig. 2(a), Fig. 3(a) and Fig. 4(a) correspond to the simulation results of Table 1. Fig. 2(b), Fig. 3(b) and Fig. 4(b) correspond to the simulation results of Table 2. Fig. 2(c), Fig. 3(c) and Fig. 4(c) correspond to the simulation results of Table 3.

Table 1 Coordinates of the station with a baseline length of 10 km km

Cloth stand shape	Master station coordinate	Auxiliary station 1 coordinate	Auxiliary station 2 coordinate	Auxiliary station 3 coordinate
Diamond	(100,100,100.1)	(100,110,100)	(91.34,105,100)	(108.66,105,100)
T-type	(100,100,100.1)	(90,100,100)	(110,100,100)	(100,90,100)
Y-type	(100,100,100.1)	(91.34,105,100)	(108.66,105,100)	(100,90,100)

Table 2 Coordinates of the station with a baseline length of 20 km km

Cloth stand shape	Master station coordinate	Auxiliary station 1 coordinate	Auxiliary station 2 coordinate	Auxiliary station 3 coordinate
Diamond	(100,100,100.1)	(100,120,100)	(82.68,110,100)	(117.32,110,100)
T-type	(100,100,100.1)	(80,100,100)	(120,100,100)	(100,80,100)
Y-type	(100,100,100.1)	(82.68,110,100)	(117.32,110,100)	(100,80,100)

Table 3 Coordinates of the station with a baseline length of 30 km km

Cloth stand shape	Master station coordinate	Auxiliary station 1 coordinate	Auxiliary station 2 coordinate	Auxiliary station 3 coordinate
Diamond	(100,100,100.1)	(100,130,100)	(74.02,115,100)	(125.98,115,100)
T-type	(100,100,100.1)	(70,100,100)	(130,100,100)	(100,70,100)
Y-type	(100,100,100.1)	(74.02,115,100)	(125.98,115,100)	(100,70,100)

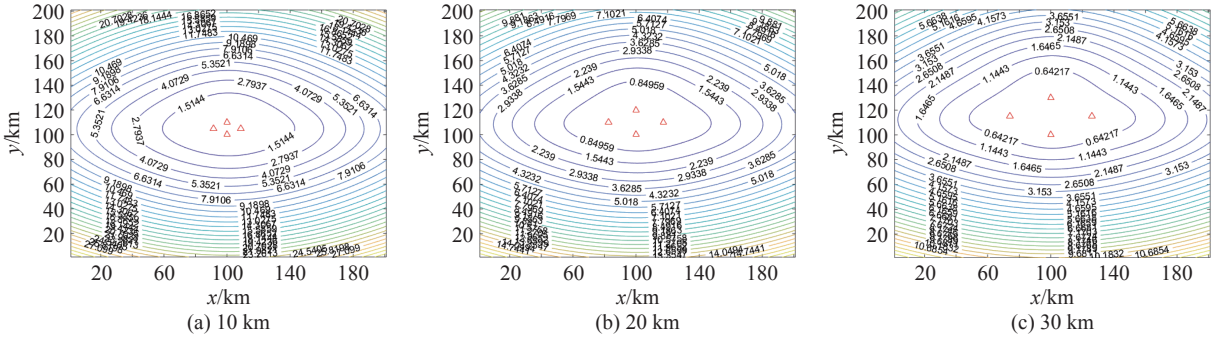

(a) 10 km (b) 20 km (c) 30 km

Fig. 2 Diamond cloth station positioning error

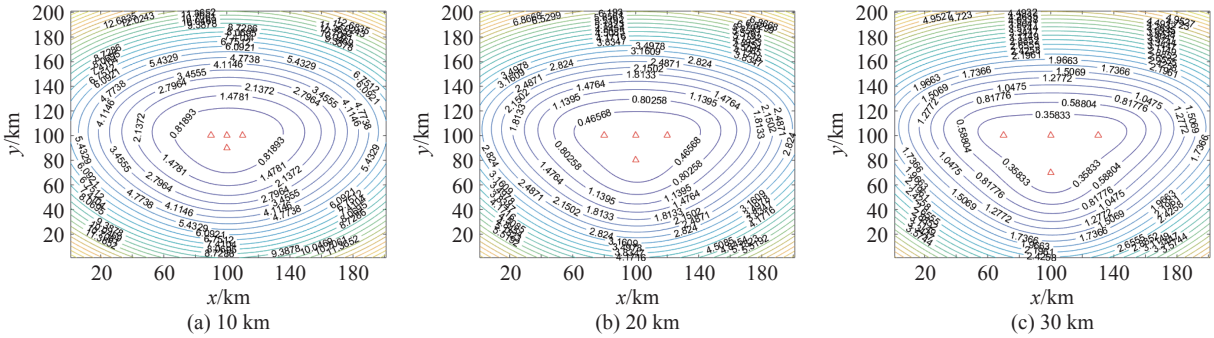

(a) 10 km (b) 20 km (c) 30 km

Fig. 3 T-type station positioning error

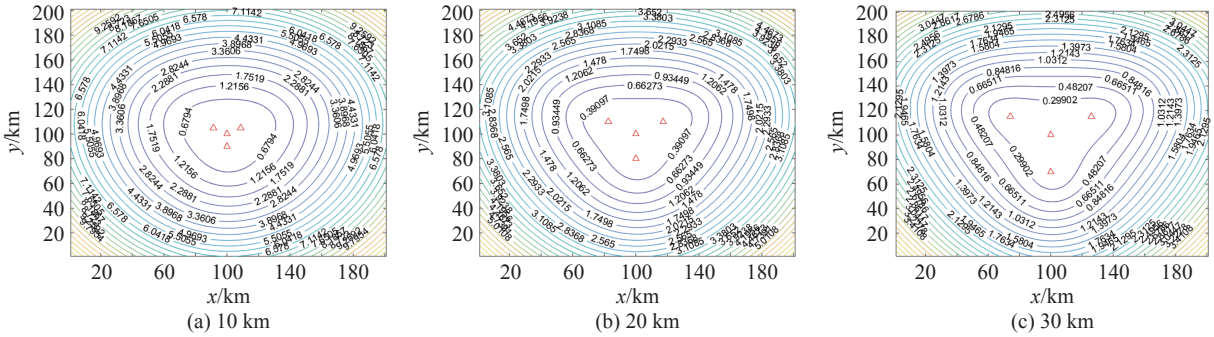

(a) 10 km (b) 20 km (c) 30 km

Fig. 4 Y-type station positioning error

Analyzing the positioning results, we can draw the following conclusions:

(i) The positioning accuracy has a positive correlation with the baseline length. The longer the baseline length, the higher the positioning accuracy. The main reason for this phenomenon is that with the same station layout and

target position, a poor baseline length can obtain a large time difference measurement value. When the time measurement error is the same, the ratio between the time measurement error and the measurement value becomes smaller, which indirectly improves the time difference measurement accuracy, and the positioning accuracy is correspondingly improved.

(ii) The positioning accuracy is related to the location of the site and the target. The further away the target is from the main station, the lower the positioning accuracy.

(iii) The positioning accuracy under the diamond-shaped cloth station is lower than that of the other two kinds of cloth station methods, and the positioning accuracy in the x-axis direction is lower than that in the y-axis direction.

(iv) Under the T-type station, the distribution of positioning accuracy is more uniform when the baseline length is 10 km. As the baseline length increases, the positioning accuracy in the y-axis direction is better than that in the x-axis direction.

(v) The positioning accuracy under the Y-type distribution station is higher than the other two distribution methods, and the distribution of positioning accuracy is more uniform, which is suitable for performing global search tasks.

4. Track optimization

TDOA positioning accuracy is mainly related to the following factors: the geometric position between the target radiation source and each UAV base station, the site error TDOA measurement error, etc., among which the geometric position relationship between the target radiation source and each UAV base station has a larger impact on positioning accuracy [36]. Therefore, for the positioning and tracking of moving targets, the real-time planning of the movement track of the UAV base station appears to be particularly important.

4.1 D-optimality criteria

The D-optimality criterion [37] is used to minimize the area of the confidence region corresponding to the estimated parameters. Compared with the A-optimality criterion [38], the D-optimality criterion directly maximizes the determinant of the Fisher information matrix [39]. Therefore, the stability of D-optimality criterion is the best, and it is not easy to be affected by the change of objective function parameters and non-linear transformation, and the process of analysis and solution is simple. Fig. 5 shows the geometrical schematic diagram of positioning. In the figure, $\boldsymbol{p}=[x,y]^{\mathrm{T}}$ is the position of the target radiation source, and $\boldsymbol{q}_i=[x_i,y_i]^{\mathrm{T}}$ is the position of the ith base station. To simplify the problem, it is assumed that the reference base station is located at the origin of the rectangular coordinate system, l_i and α_i are respectively the distance and the azimuth from the ith base station to the reference base station.

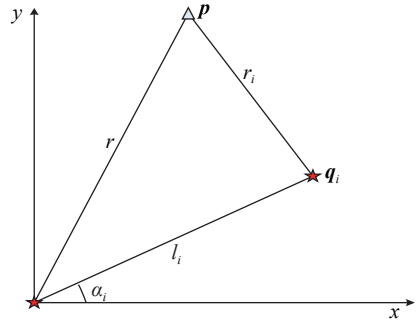

Fig. 5 Positioning geometric relationship

Therefore, there is the following relationship: $x_i=l_i\cos\alpha_i$, $y_i=l_i\sin\alpha_i$,

$$t_{i1}^0=\frac{1}{c}(r_i-r)=\frac{1}{c}\left(\sqrt{(x-l_i\cos\alpha_i)^2+(y-l_i\sin\alpha_i)^2}-\sqrt{x^2+y^2}\right) \tag{21}$$

where c is the velocity of electromagnetic wave propagation. The following conclusions can be drawn:

$$\begin{cases}\dfrac{\partial t_{i1}^o}{\partial x}=\dfrac{1}{c}\left[\dfrac{-l_i\cos\alpha_i}{r_i}+x\left(\dfrac{1}{r_i}-\dfrac{1}{r}\right)\right]\\ \dfrac{\partial t_{i1}^o}{\partial y}=\dfrac{1}{c}\left[\dfrac{-l_i\sin\alpha_i}{r_i}+y\left(\dfrac{1}{r_i}-\dfrac{1}{r}\right)\right]\end{cases}. \tag{22}$$

When locating a far-field target, there is $r_i\approx r$, therefore[40],

$$\begin{cases}\dfrac{\partial t_{i1}^o}{\partial x}=-\dfrac{l_i\cos\alpha_i}{cr}\\ \dfrac{\partial t_{i1}^o}{\partial y}=-\dfrac{l_i\sin\alpha_i}{cr}\end{cases}. \tag{23}$$

The Fisher information matrix of the target position error can be obtained from (1) as

$$\boldsymbol{J}=\boldsymbol{G}^{\mathrm{T}}\boldsymbol{\Omega}^{-1}\boldsymbol{G}=\left[\frac{\partial t^0}{\partial x},\frac{\partial t^0}{\partial y}\right]^{\mathrm{T}}\boldsymbol{\Omega}^{-1}\left[\frac{\partial t^0}{\partial x},\frac{\partial t^0}{\partial y}\right]. \tag{24}$$

From (3):

$$\boldsymbol{\Omega}^{-1}=\frac{1}{(n+1)\sigma^2}[(n+1)\boldsymbol{I}-\boldsymbol{\Phi}]. \tag{25}$$

Let $\boldsymbol{J}=\begin{bmatrix}J_{11} & J_{12}\\ J_{21} & J_{22}\end{bmatrix}$, where J_{11}, J_{12}, J_{21} and J_{22} are as follows:

$$J_{11}=\frac{1}{(n+1)\sigma^2}\frac{1}{c^2r^2}\left[(n+1)\sum_{i=1}^{n}l_i^2\cos^2\alpha_i-\left(\sum_{i=1}^{n}l_i\cos\alpha_i\right)^2\right] \tag{26}$$

$$J_{12}=J_{21}=\frac{1}{(n+1)\sigma^2}\frac{1}{c^2r^2}\left[(n+1)\sum_{i=1}^{n}l_i^2\cos\alpha_i\sin^2\alpha_i-\left(\sum_{i=1}^{n}l_i\sin\alpha_i\right)\left(\sum_{i=1}^{n}l_i\cos\alpha_i\right)\right] \tag{27}$$

$$J_{22}=\frac{1}{(n+1)\sigma^2}\frac{1}{c^2r^2}\left[(n+1)\sum_{i=1}^{n}l_i^2\sin^2\alpha_i-\left(\sum_{i=1}^{n}l_i\sin\alpha_i\right)^2\right]. \tag{28}$$

Therefore, the objective function of D-optimality is

$$\arg\max\ \det(\boldsymbol{J})=J_{11}J_{22}-J_{12}J_{21}. \tag{29}$$

4.2 Track optimization

The derivation process of the D-optimality criterion is given in Section 4.1. The optimal trajectory of the UAV is the maximum value of the Fisher matrix determinant that moves the UAV toward the next moment. However, in practical applications, considering the maximum turning angle of the UAV $\theta_{\max}$ and the speed of movement, the conditions for the optimal configuration of the target positioning cannot be achieved in a short time. Therefore, at each track node, a sector is given with an angle range of $2\theta_{\max}$ to traverse all the angles of the sector and filter out the angle corresponding to the maximum value of the Fisher information matrix determinant, which is the heading of the UAV at the next moment. Fig. 6 shows the schematic diagram of flight path planning for UVA swarm.

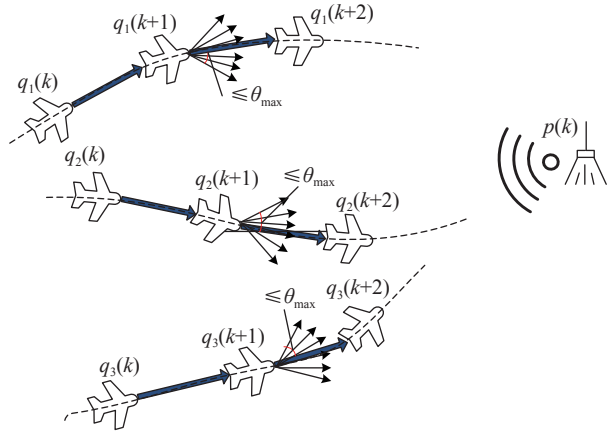

Fig. 6 Schematic diagram of flight path planning for UAV cluster

To sum up, the data processing flow of UAV track planning based on D-optimality is as follows.

Step 1 Give the position coordinates k of each UAV at the time $\boldsymbol{Q}_k=[\boldsymbol{q}_1(k),\boldsymbol{q}_2(k),\cdots,\boldsymbol{q}_n(k)]^{\mathrm{T}}$, the time difference positioning measurement value $\boldsymbol{t}_k$;

Step 2 Solve the distance-dependent noise σ^2;

Step 3 Use the Chan algorithm to solve the estimated position $\hat{\boldsymbol{p}}_k$ of the target through two weighted least squares;

Step 4 Calculate the Fisher information matrix and solve the objective function;

Step 5 Obtain the optimal angle of the UAV flying at the next moment.

Fig. 7 shows the positroning and track planning process.

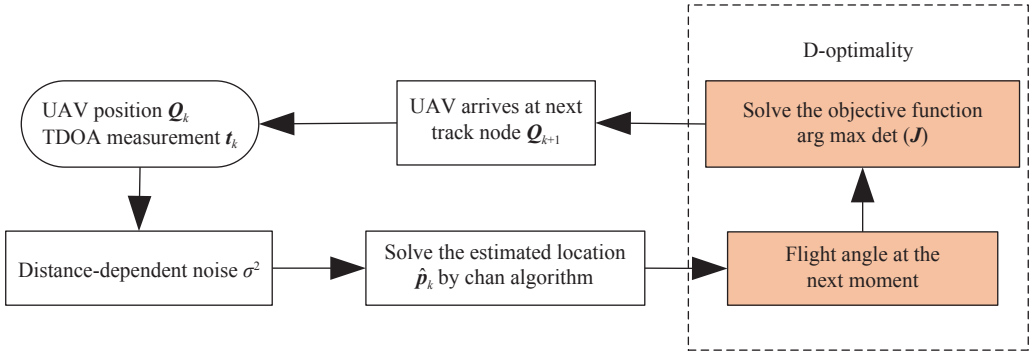

Fig. 7 Positioning and track planning process

5. Simulation

Assume that four UAVs are used to locate the target. The initial state of the UAV is $\boldsymbol{q}_1(1)=[0,-8\,000,0,-5\,000]^{\mathrm{T}}$ km, $\boldsymbol{q}_2(1)=[0,-7\,500,0,-5\,000]^{\mathrm{T}}$ km, $\boldsymbol{q}_3(1)=[0,-7\,500,0,-6\,000]^{\mathrm{T}}$km, $\boldsymbol{q}_4(1)=[0,-7\,000,0,-6\,000]^{\mathrm{T}}$km, and the initial time is to fly along the y-axis. The fixed flight speed $v_u=70$ m/s, the maximum turning angle $\theta_{\max}=10^{\circ}$ km, the sampling interval $T=1s$, and $\mathrm{SNR}_0=30$ dB. The real position of the stationary target is $[0,0,0,0]^{\mathrm{T}}$, 100 Monte-Carlo simulations are performed, and the following results are obtained.

5.1 Stationary target

Fig. 8 (a) is the UAV path and positioning results optimized by the D-optimality criterion, Fig. 8 (b) is the path and positioning results of the UAV flying in a fixed path, Fig. 8 (c) is the optimized path and positioning under the fixed path error comparison, and Fig. 8 (d) is the angle change of each UAV under the optimized path. From

Fig. 8 (a) and Fig. 8 (d), it can be seen that UAV2 and UAV3 always fly towards the target when they are far away from the target, and when they are closer to the target, the flight angle changes greatly in order to arrange the station reasonably. UAV1 and UAV4 fly to both sides. Comparing with Fig. 8 (a) and Fig. 8 (b), the positioning results under the fixed configuration flight are more dispersed. Therefore, in Fig. 8 (c), under the optimized path, the positioning error is lower than that in the fixed configuration, and the convergence speed is faster.

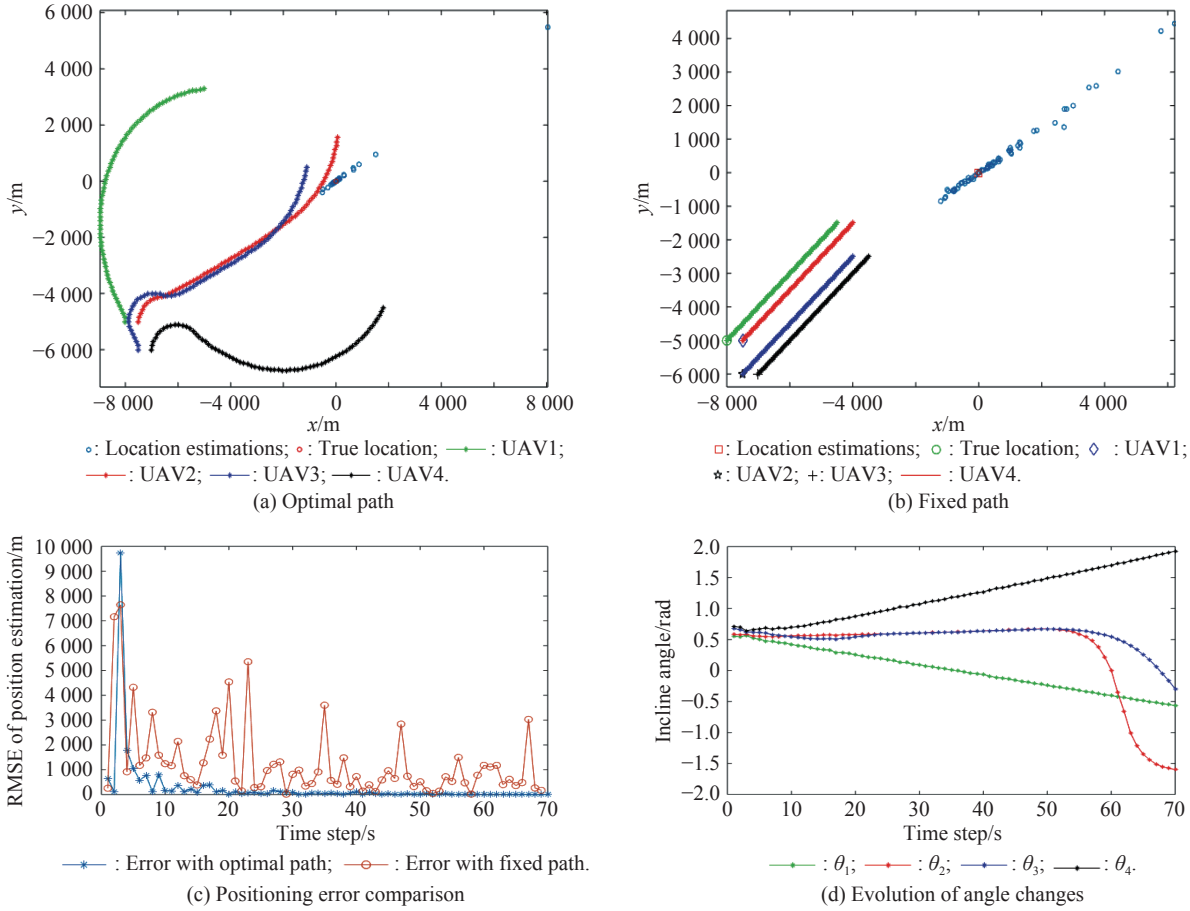

Fig. 8 Positioning result of stationary target

5.2 Moving target

The motion state of the target is divided into the uniform straight line, the uniformly accelerating straight line, and the uniformly turning motion. The initial positions are $\left[0,50\sqrt{3},0,50\sqrt{3}\right]^{\mathrm{T}}$ km, the target's uniform flying speed $v_t = 50$ m/s, the initial speed $v_{t_0} = 3$ m/s, acceleration $a = 3$ m/s^2 during uniform acceleration, and the state transition matrix for uniform turning is

$$\boldsymbol{F}_k = \begin{bmatrix} 1 & \dfrac{\sin(\omega T)}{\omega} & 0 & -\dfrac{(1-\cos(\omega T))}{\omega} \\ 0 & \cos(\omega T) & 0 & -\sin(\omega T) \\ 0 & \dfrac{(1-\cos(\omega T))}{\omega} & 1 & \dfrac{\sin(\omega T)}{\omega} \\ 0 & \sin(\omega T) & 0 & \cos(\omega T) \end{bmatrix},$$

where ω=0.5.

5.2.1 Target at constant speed

As shown in Fig. 9 (a) and Fig. 9 (d), each UAV tries to fly away from each other as far as possible. After a rough judgment of the target position, UAV2 and UAV3 begin to fly in the direction of the target, shorten the distance with the target and improve the positioning accuracy. UAV1 and UAV3 are scattered in a direction perpendicular to UAV2 and UAV4. This phenomenon occurs because the longer the baseline of the station, the higher the accuracy of positioning. Comparing the distribution of the positioning results in Fig. 9 (a) and Fig. 9 (b), it can be concluded that the optimized positioning of the target for the uniformly-linear motion of the target is mainly distributed around the actual position of the target. Results are more scattered. Fig. 9 (c) compares the positioning errors of the two paths.

It can be concluded that the positioning error of the optimized path is always lower than that of the fixed path.

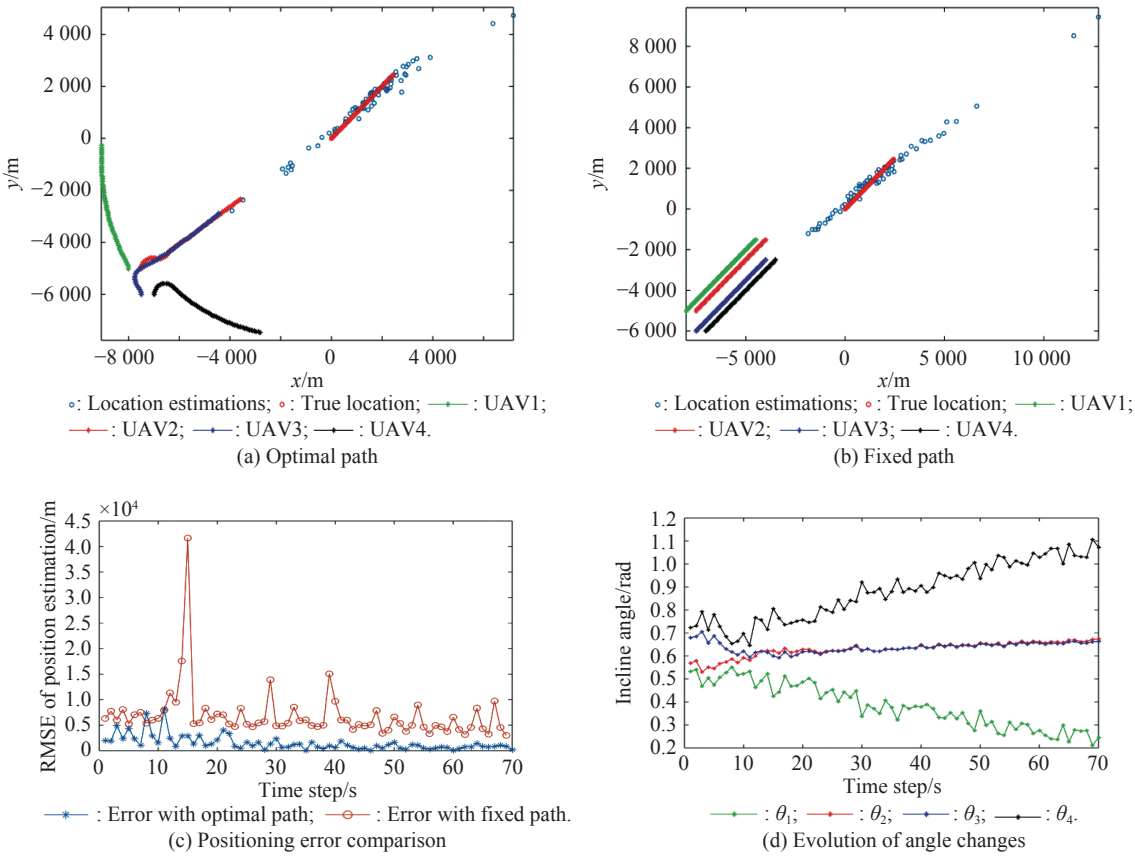

Fig. 9 Positioning results under uniform motion

5.2.2 Target accelerating uniformly

Fig. 10 (a) and Fig. 10 (d) reflect the changes in the flight path and angle of the UAV to a uniformly accelerated moving target under D-optimality. Compared with Fig. 8, the UAV always disperses in a direction away from each other. The angle change at the initial moment is also larger. As the positioning time passes, the angle change gradually becomes smaller. This is because the distance between the target and the UAV is relatively large when the target is performing uniformly accelerated linear motion. As a result of positioning, a longer baseline length is needed between the UAV base stations to accurately locate the target. Because it is assumed that the UAVs are flying in the y-axis direction at the initial moment, UAV3 is limited by the maximum turning angle and cannot immediately turn to the angle of scattered flying with other UAVs. Therefore, a larger arc is used to adjust the flight direction. Fig. 10 (c) clearly reflects the positioning error of the UAV in two paths of the flight. When the target performs uniformly accelerated linear motion, the error of the optimized path is also lower than the positioning error of the fixed path.

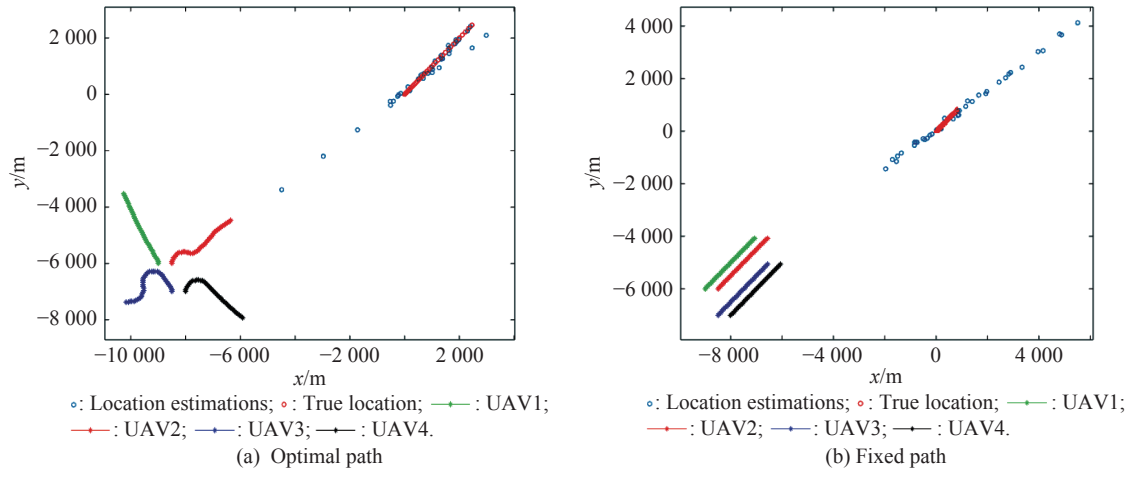

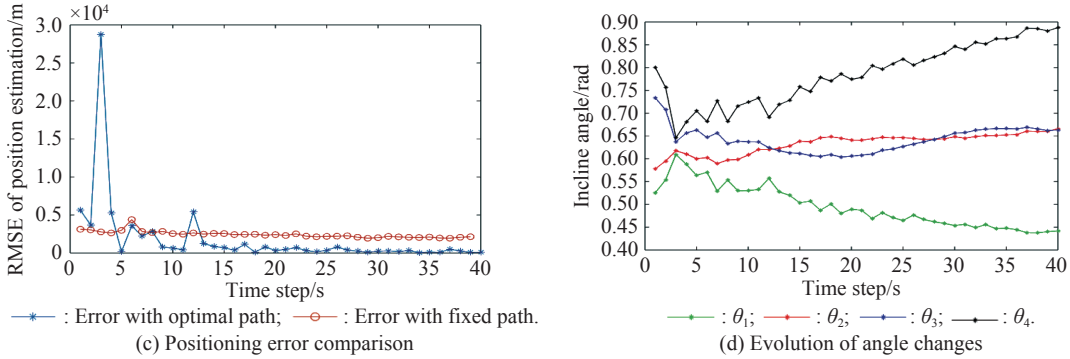

(c) Positioning error comparison (d) Evolution of angle changes

Fig. 10 Positioning results under uniform acceleration

5.2.3 Target turning at a constant speed

When the target makes a uniform turning movement, compared with the previous two types of target movement, the distance between the UAV and the target does not always increase. UAV2 and UAV3 are flying toward the target, and the distance to the target is reduced. UAV1 and UAV4 fly to both sides, increasing the baseline length of the UAV deployment station and improving the positioning accuracy. It can be obtained from Fig. 11 (c) that the positioning error and convergence speed under the optimized path are lower than the positioning error under the fixed path flight. When flying under the fixed path, the positioning error first decreases and then increases slightly. This is because when the target makes a uniform turning movement, the target is flying towards the UAV for a period of time, the distance between the UAV and the target decreases, and the positioning error increases as the target flies away from the UAV. However, the positioning error under the optimized path has been relatively stable, and it is not easily affected by the target motion state.

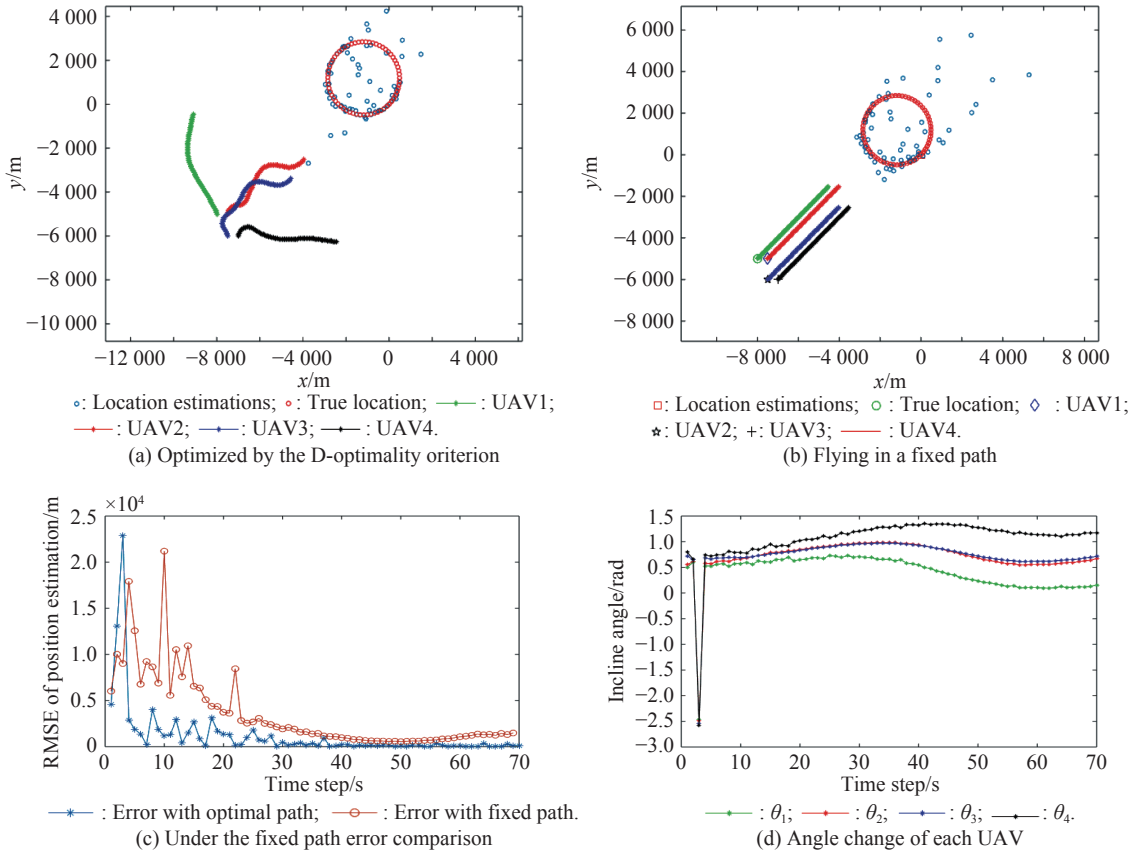

(a) Optimized by the D-optimality oriterion (b) Flying in a fixed path

(c) Under the fixed path error comparison (d) Angle change of each UAV

Fig. 11 Positioning results under a uniform turning motion

6. Conclutions

In this paper, UAV swarm is used to locate and track the moving targets. A TDOA positioning model and a model of the variation of the error variance with the received SNR are established, and the positioning accuracy of time difference positioning is analyzed by using GDOP. The D-optimality criterion under this model is derived theoretically. The Chan algorithm is used to locate the target, and the maximum value of the Fisher information matrix determinant is used as the objective function to carry out real-time planning of the trajectory of the UAV. Simulation analysis shows that the positioning accuracy of the target can be effectively improved by planning the path of the UAV swarm, and the target's positioning accuracy after the optimized path is higher than the fixed path under the three motion states set. The positioning accuracy indicates that the path optimized by the D-optimality criterion is more adaptive to change in the target position.

This paper mainly considers one-step path optimization. If multiple paths are used to predict the path in advance, it will have a better positioning effect, but at the same time, it will increase the computational complexity and increase the path optimization time, which is a challenge to real-time performance. Subsequent work will focus on reducing the computational complexity and achieving multi-step path prediction.

References

[1] GAO Y, LI D S, CHENG Z X. UAV distributed swarm situation awareness model. Journal of Electronics & Information Technology, 2018, 40(6): 1271–1278. (in Chinese)

[2] LIANG X L, ZHANG J Q, LU N. UAV swarm. Xi'an: Northwestern Polytechnical University Press, 2018. (in Chinese)

[3] PHAM H, LA H, FEIL-SEIFER D, et al. Autonomous UAV navigation using reinforcement learning. Ithaca: Cornell University, 2018.

[4] NGUYEN N H, DOGANCY K. Closed-form algebraic solutions for angle-of-arrival source localization with Bayesian priors. IEEE Trans. on Wireless Communications, 2019, 18(8): 3827–3842.

[5] WANG Y, HO D. Unified near-field and far-field localization for AOA and hybrid AOA-TDOA positionings. IEEE Trans. on Wireless Communications, 2018, 17(2): 1242–1254.

[6] TOMIC S, BEKO M, DINIS R, et al. A closed-form solution for RSS/AoA target localization by spherical coordinates conversion. IEEE Wireless Communications Letters, 2016, 5(6): 680–683.

[7] RUI L, HO K C. Elliptic localization: performance study and optimum receiver placement. IEEE Trans. on Signal Processing, 2014, 62(18): 4673–4688.

[8] TOMIC S, BEKO M, DINIS R, et al. A robust bisection-based estimator for TOA-based target localization in NLOS environments. IEEE Communications Letters, 2017, 21(11): 2488–2491.

[9] D'AMICO A A, TAPONECCO L, MENGAALI U. Ultra-wideband TOA estimation in the presence of clock frequency offset. IEEE Trans. on Wireless Communications, 2013, 12(4): 1606–1616.

[10] GHOLAMI M R, GEZICI S, STROM E G, et al. TDOA based positioning in the presence of unknown clock skew. IEEE Trans. on Communications, 2013, 61(6): 2522–2534.

[11] WANG G, HO K C. Convex relaxation methods for unified near-field and far-field TDOA-based localization. IEEE Trans. on Wireless Communications, 2019, 18(4): 2346–2360.

[12] JIN B N, XU X S, ZHANG T. Robust time-difference-of-arrival (TDOA) localization using weighted least squares with cone tangent plane constraint. Sensors, 2018, 18(3): 778.

[13] TOMIC S, BEKO M, DINIS R, et al. Distributed RSS-based localization in wireless sensor networks based on second-order cone programming. Sensors , 2014, 14(10): 18410–18432.

[14] KHAN M A, SAEED N, AHMAD A W, et al. Location awareness in 5G networks using RSS measurements for public safety applications. IEEE Access, 2017, 5: 21753–21762.

[15] TOMIC S, BEKO M, DINIS R, et al. RSS-based localization in wireless sensor networks using convex relaxation non-cooperative and cooperative schemes. IEEE Trans. on Vehicular Technology, 2015, 64(5): 2037–2050.

[16] ZHU G H, FENG D Z, XIE H, et al. An approximately efficient bi-iterative method for source position and velocity estimation using TDOA and FDOA measurements. Signal Processing, 2016, 125: 110–121.

[17] FOY W H. Position-location solutions by Taylor-series estimation. IEEE Trans. on Aerospace Electronic Systems, 2007, 12(2): 187–194.

[18] WANG J, GUO J. Research on the base station calibration of multi-station and time-sharing measurement based on hybrid genetic algorithm. Measurement, 2016, 94: 139–148.

[19] CHAN Y T, HO K C. A simple and efficient estimator for hyperbolic location. IEEE Trans. on Signal Processing, 1994, 42(8): 1905–1915.

[20] SCHAU H C, ROBINSON A Z. Passive source localization employing intersecting spherical surfaces from time-of-arrival differences. IEEE Trans. on Acoustics, Speech, and Signal Processing, 2003, 35(8): 1223–1225.

[21] MALANOWSKI M, KULPA K. Two methods for target localization in multistatic passive radar. IEEE Trans. on Aerospace Electronic Systems, 2012, 48(1): 572–580.

[22] WANG P W. Research and application on the key technologies for TDOA passive source localization. Xi'an: Xidian University, 2018. (in Chinese)

[23] WANG Y, HO K C. TDOA positioning irrespective of source range. IEEE Trans. on Signal Processing, 2017, 65(6): 1447–1460.

[24] WANG G, CHEN H. An importance sampling method for TDOA-based source localization. IEEE Trans. on Wireless Communications, 2011, 10(5): 1560–1568.

[25] FREW E W, DIXON C, ARGROWB, et al. Radio source localization by a cooperating UAV team. Proc. of the AIAA Infotech @ Aerospace, 2005: AIAA 2005 – 6903.

[26] SEMPER S R, CRASSIDIS J L. Decentralized geolocation

and optimal path planning using limited UAVs. Proc. of the IEEE 12th International Conference on Information Fusion, 2009: 355 – 362.

[27] MORENO-SALINAS D, PASCOAL A, ALMANSA J A. Sensor networks for optimal target localization with bearings-only measurements in constrained three-dimensional scenarios. Sensors, 2013: 13(8): 10386–10417.

[28] SONIA M, BULLO F. Optimal sensor placement and motion coordination for target tracking. Automatica , 2006, 42(4): 661–668.

[29] KAUNE R, CHARLISH A. Online optimization of sensor trajectories for localization using TDOA measurements. Proc. of the IEEE 16th International Conference on Information Fusion, 2013: 484−491.

[30] PEREZ-RAMIREZ J, BORAH D K, VOELZ D G. Optimal 3-D landmark placement for vehicle localization using heterogeneous sensors. IEEE Trans. on Vehicular Technology, 2013, 62(7): 2987–2999.

[31] LANZISERA S, ZATS D, PSITER K S J. Radio frequency time-of-flight distance measurement for low-cost wireless sensor localization. IEEE Sensors Journal, 2011, 11(3): 837–845.

[32] GHABCHELOO R, AGUIAR A P, PASCOL A, et al. Coordinated path-following in the presence of communication losses and time delays. SIAM Journal on Control & Optimization, 2009, 48(1): 234–265.

[33] KAUNE R, HORST J, KOCH W. Accuracy analysis for TDOA localization in sensor networks. Proc. of the IEEE 14th International Conference on Information Fusion, 2011: 1647–1654.

[34] SHARP I, YU K. GDOP analysis for positioning design. Singapore: Springer, 2019.

[35] LAVETIA G, RAO G S, CHAITANYA D E, et al. TDOA measurement based GDOP analysis for radio source localization. Procedia Computer Science, 2016, 85: 740–747.

[36] SUN H. Research and implementation of multi station passive TDOA location algorithm. Harbin: Harbin Engineering University, 2017. (in Chinese)

[37] UCINSKI D. Optimal measurement methods for distributed parameter system identification. Boca Raton: CRC Press, 2004.

[38] DOGANCAY D, HMAM H. On optimal sensor placement for time difference of arrival localization utilization uncertainty minimization. Proc. of the 17th European Signal Processing Conference, 2009: 1136−1140.

[39] MERENO-SALINAS D, PASCOAL A, ARANDA J. Optimal sensor placement for acoustic underwater target positioning with range-only measurements. IEEE Journal of Oceanic Engineering, 2016, 41(3): 620–643.

[40] MERENO-SALINAS D, PASCOAL A, ARANDA J A. Optimal sensor placement for underwater positioning with uncertainty in the target location. Proc. of the IEEE International Conference on Robotics and Automation, 2011: 2308−2314.

Biographies

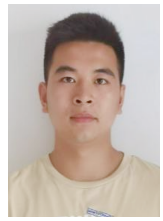

ZHOU Ronghua was born in 1996. He received his B.E. degree in radar engineering from Air Force Early Warning Academy, Wuhan, China. His research interests are swarm intelligence, blind source separation, and intelligent optimization. He has published more than two journal papers as the major author, one of which is retrieved by SCI/EI.
E-mail: 915216235@qq.com

SUN Hemin was born in 1972. He received his B. E. degree in radar engineering, and M. E. degree in weapon systems and applications from Air Force Early Warning Academy, Wuhan, China. His current research interests are radar engineering and intelligence processing. He has published more than 30 journal papers as the major author.
E-mail: skylar1013@126.com

LI Hao was born in 1981. He received his Ph.D. degree in electronic science and technology from Air Force Engineering University in 2017, Xi'an, China. His current research interests are swarm intelligence, UAV swarm, intelligence systems and signal processing. He has published more than 30 journal papers as the major author, among them, 20 articles are retrieved by SCI/EI.
E-mail: Afeu_li@163.com

LUO Weilin was born in 1995. He received his B. E. degree in communication engineering from Xidian University in 2018, Xi'an, China. His research interests are swarm intelligence, blind source separation, intelligent optimization. He has published more than four journal papers as the major author, one of which is retrieved by SCI/EI.
E-mail: 810953644@qq.com